Dalton Transactions

ROYAL SOCIETY OF CHEMISTRY

FRONTIER

View Article Online
View Journal | View Issue

Cite this: *Dalton Trans.*, 2024, **53**, 12034

Galloborates as ultraviolet nonlinear optical crystals: advances and perspectives

Jing-Yi Lu, Yangfeifei Ou, Cong-Cong Jin* and Jian-Wen Cheng *

Received 24th April 2024,
Accepted 14th June 2024

DOI: 10.1039/d4dt01206b

rsc.li/dalton

Metal borates are excellent source materials for exploring short-wavelength nonlinear optical (NLO) crystals. Galloborates show rich structural chemistry with various coordination configurations of Ga cation and B–O anionic units and are suitable candidates as ultraviolet NLO crystals. Up to now, the shortest cut-off edge of galloborates was reported to be down to 190 nm in $KCs_2Ga(B_5O_{10})(OH)$, while the largest second harmonic generation (SHG) effect of galloborates was reported to be up to 4.6 times that of KH_2PO_4 (KDP) in $Na_5Ga[B_7O_{12}(OH)]_2{\cdot}2B(OH)_3$. Herein, we give a detailed summary of the recent progress in NLO inorganic galloborates, where these galloborates are grouped into two types in terms of their compositions: (1) alkali/alkaline earth metal galloborates and (2) alkali/alkaline earth metal galloborate halides. We discuss their structural features, band gaps, and SHG intensities. Finally, we give future perspectives in this field.

1. Introduction

Nonlinear optical (NLO) materials are widely used to convert a specific wavelength of light to half its original.[1–17] The discovery of LiB_3O_5 (LBO), β-BaB_2O_4 (β-BBO), and $KBe_2BO_3F_2$ (KBBF) in borate systems greatly accelerated the development of ultraviolet (UV) and deep-UV NLO crystals.[18–20] These crystals are used to obtain coherent UV and deep-UV light *via* the cascaded frequency conversion of Nd:YAG lasers (1064 nm). According to the anionic group theory, $[B_3O_7]$, $[B_3O_6]$, and $[BO_3]$ are the NLO-active functional units in LBO, β-BBO, and KBBF, while Li, Ba, and K cations contribute less. To date, a large number of alkali and alkaline earth metal borate-based NLO crystals have been found.[21–27] One very recent example is $Ba_4B_{14}O_{25}$, which shows a highly polymeric three-dimensional geometry with a closed-loop anionic framework constructed by the fundamental building blocks (FBBs) $[B_{14}O_{33}]$, and it is a deep-UV transparent NLO crystal with strong second harmonic generation (SHG) (3.0 × KH_2PO_4, KDP).[28] Generally, a perfect UV or deep-UV NLO crystal should possess certain characteristics including a wide optical transparency window, large NLO coefficient, and moderate birefringence, and it should be easy to grow large single crystals.

The modification of the borate anionic unit is an effective method to find new NLO crystals.[29] Fluorooxoborates are considered the best candidates for the next generation of deep-UV NLO materials.[30] Fluorinated $[BO_xF_{4-x}]$ (x = 1–3) units show larger polarizability anisotropy than that of $[BO_4]$, and the higher electronegativity of fluorine ions usually leads to blue-shifted cut-off edges in fluorooxoborates. To date, more than 80 examples of fluorooxoborates have been found, among which more than one-third are crystallized in noncentrosymmetric space groups.[31] $NH_4B_4O_6F$ displays a wave-like layer constructed from a corner-sharing anionic structural motif of $[B_4O_8F]$, and it is an excellent deep-UV NLO crystal with a very short cut-off edge (156 nm) and large NLO effect (3.0 × KDP).[32] In addition, the newly discovered sp hybridized linear $[BO_2]$ in synthetic borates shows a larger polarizability anisotropy than that of $[BO_3]$ and $[BO_4]$ units according to the theoretical analyses.[33] This functional unit may provide more opportunities to discover other NLO and birefringent materials.

The substitution or partial substitution of alkali and alkaline earth metal cations by other metal cations in borates lead to a new family of borates with excellent properties.[34,35] A larger band gap may be achieved by partially eliminating the dangling bond of the terminal O atoms, as evidenced by $Zn_2BO_3(OH)$,[36] $Cs_3Zn_6B_9O_{21}$,[37] β-$Rb_2Al_2B_2O_7$,[38] and $CsAlB_3O_6F$.[39] $Zn_2BO_3(OH)$ shows a KBBF-like structure by replacing $[BeO_3F]$ with $[ZnO_3(OH)]$ and exhibits a short UV cut-off edge (204 nm) and a SHG response of 1.5 × KDP.[36] Galloborates are suitable candidates for UV NLO crystals due to their rich structures, wide transmittance, and excellent optical properties. To date, 12 NLO inorganic galloborates have been reported, and the shortest cut-off edge of galloborates was reported to be down to 190 nm in $KCs_2Ga(B_5O_{10})(OH)$,[40] while the largest SHG effect of galloborates was reported to be up to 4.6 × KDP in $Na_5Ga[B_7O_{12}(OH)]_2{\cdot}2B(OH)_3$.[41] In this frontier article, we review the recent progress in NLO galloborates. These galloborates are divided into two types in terms of their chemical compositions:

Key Laboratory of the Ministry of Education for Advanced Catalysis Materials, Institute of Physical Chemistry, Zhejiang Normal University, Jinhua, Zhejiang 321004, China. E-mail: jincongcong@zjnu.edu.cn, jwcheng@zjnu.cn

Table 1 Noncentrosymmetric galloborates and their properties

Compounds	Space groups	SHG intensities	Band gaps	Ref.
$Rb_2Ga(B_5O_{10})(H_2O)_4$	$C222_1$	1.0 × KDP	3.54 eV	43
$KCs_2Ga(B_5O_{10})(OH)$	$I\bar{4}2d$	1.4 × KDP	6.30 eV	40
$Ba_4Ga[B_{10}O_{18}(OH)_5](H_2O)$	Cc	0.2 × KDP	4.12 eV	46
$Na_4Ga_3B_4O_{12}(OH)$	$F\bar{4}3c$	0.1 × KDP	4.90 eV	47
$Na_5Ga[B_7O_{12}(OH)]_2{\cdot}2B(OH)_3$	$C2$	4.6 × KDP	3.90 eV	41
$Ba_3Ga_2[B_3O_6(OH)]_2[B_4O_7(OH)_2]$	$Fdd2$	3.0 × KDP	5.0 eV	48
$K_2Ba_4Li_2Ga_4B_6O_{21}$	$P\bar{6}2c$	0.5 × KDP	5.49 eV	54
$Ba_2GaB_4O_9Cl$	$P4_2nm$	1.0 × KDP	N/A	50
$NaBa_4(GaB_4O_9)_2Cl_3$	$P4_2nm$	1.5 × KDP	3.76 eV	49 and 53
$NaBa_4(GaB_4O_9)_2Br_3$	$P4_2nm$	1.1 × KDP	3.71 eV	53
$K_3Ba_3Li_2Ga_4B_6O_{20}F$	$P\bar{6}2c$	0.7 × KDP	>6.20 eV	55
$Rb_3Ba_3Li_2Ga_4B_6O_{20}F$	$P\bar{6}2c$	0.5 × KDP	>6.20 eV	55

(1) alkali/alkaline earth metal galloborates, and (2) alkali/alkaline earth metal galloborate halides. The chemical formulas, space groups, SHG intensities, and band gaps of these galloborates are summarized in Table 1. We also give the further perspectives and challenges in this field.

2. Alkali/alkaline earth metal galloborates

$K_2Ga(B_5O_{10})(H_2O)_4$ was synthesized by Liu *et al. via* a mild solvothermal method in 2007. It was the first reported member of borates featuring a three-dimensional zeolite-like $[GaB_5O_{10}]_\infty$ framework.[42] Liu *et al.* reported the synthesis of $K_2Ga(B_5O_{10})(H_2O)_4$ and discussed its structural features; however, they did not further study its physical properties. The $[GaB_5O_{10}]_\infty$ anionic skeletons, comprised of four-fold coordinated $[GaO_4]$ tetrahedra and $[B_5O_{10}]$ pseudo tetrahedra, are able to encapsulate guest molecules and counter cations ranging from inorganic components to organic amines. Isostructural galloborate $Rb_2Ga(B_5O_{10})(H_2O)_4$ was discovered later.[43] The similar hybrid member $(H_2EDAP)Ga(B_5O_{10})(H_2O)$ exhibited an SHG response 0.5 times that of KDP.[44] The flexibilities of the zeolite-like $[GaB_5O_{10}]_\infty$ frameworks are reflected in the tuneable sizes of their skeletons for guest encapsulation, with their changeable topologies transforming from *dia* to *und* if $[GaO_4]$ tetrahedra and $[B_5O_{10}]$ units act as 4-connected nodes.[40] $Rb_2Ga(B_5O_{10})(H_2O)_4$ and $KCs_2Ga(B_5O_{10})(OH)$ are two galloborates in this category, and they show non-isostructural anionic frameworks with different topologies. Their optical properties have been preliminarily studied.

$Rb_2Ga(B_5O_{10})(H_2O)_4$ synthesized by Mao *et al.* in 2012 crystallizes in the chiral space group of $C222_1$ (no. 20).[43] In the structure of $Rb_2Ga(B_5O_{10})(H_2O)_4$, the centred Ga cations are four-coordinated with neighbouring $[B_5O_{10}]$ FBBs (Fig. 1a), while the $[B_5O_{10}]$ FBBs share bridging μ_2-O atoms with the epitaxial Ga cations. The alternate connectivity between the $[GaO_4]$ tetrahedra and $[B_5O_{10}]$ FBBs gives rise to the three-dimensional $[GaB_5O_{10}]_\infty$ framework with the *dia* topology (Fig. 1b and c). Rb cations and guest water molecules with the

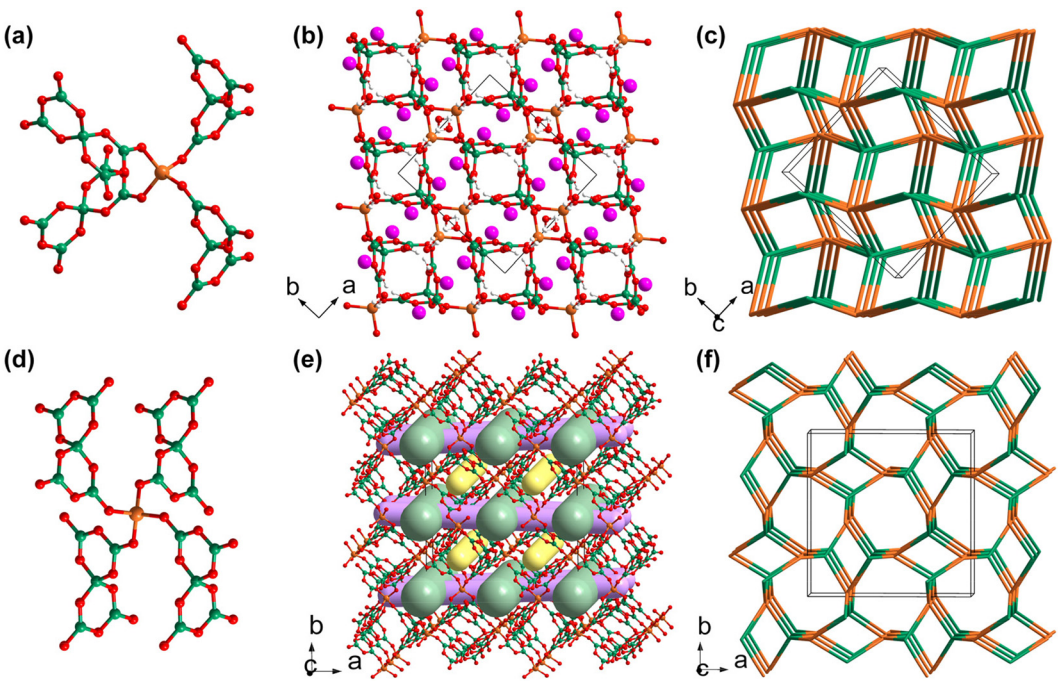

Fig. 1 (a) $[GaB_5O_{10}]$ fragment in the structure of $Rb_2Ga(B_5O_{10})(H_2O)_4$. (b) Structure of $Rb_2Ga(B_5O_{10})(H_2O)_4$. (c) The *dia* topology of the $[GaB_5O_{10}]_\infty$ anionic skeleton of $Rb_2Ga(B_5O_{10})(H_2O)_4$. (d) $[GaB_5O_{10}]$ fragment in the structure of $KCs_2Ga(B_5O_{10})(OH)$. (e) Structure of $KCs_2Ga(B_5O_{10})(OH)$ incorporating three kinds of channels. (f) The *und* topology of the $[GaB_5O_{10}]_\infty$ anionic skeleton of $Rb_2Ga(B_5O_{10})(H_2O)_4$. Rb, Ga, B, O, and H atoms are shown in rose, orange, olive, red, and white, respectively.

ratio of 1 : 2 occupy the vacancies to ensure the charge balance. The band gap of $Rb_2Ga(B_5O_{10})(H_2O)_4$ is 3.54 eV, which is slightly smaller than that of isostructural $(NH_4)_2Al(B_5O_{10})(H_2O)_4$ (3.96 eV) and $K_2Al(B_5O_{10})(H_2O)_4$ (4.45 eV). Powder SHG measurements based on Kurtz–Perry rules revealed that $Rb_2Ga(B_5O_{10})(H_2O)_4$ shows a moderate SHG intensity comparable to that of KDP, while the SHG responses of $(NH_4)_2Al(B_5O_{10})(H_2O)_4$ and $K_2Al(B_5O_{10})(H_2O)_4$ are two times that of KDP.[45] Given that $[B_5O_{10}]$ FBBs have two roughly perpendicular $[B_2O_5]$ dimers, the $[BO_3]$ triangles are naturally unable to align. The upper limit of the SHG response is restricted by the geometric configuration of $[B_5O_{10}]$ FBBs.

In 2023, Yang *et al.* used gallium isopropoxide as a gallium source and synthesized a mixed alkali metal hydrated galloborate $KCs_2Ga(B_5O_{10})(OH)$, and then immediately uncovered its potential as an NLO crystal with a deep-UV transparency window.[40] It should be noted that large amounts of galloborates and aluminoborates have been obtained under mild hydro/solvothermal condition since Yang *et al.* first proposed the use of metal isopropoxides as new sources for replacing the traditional inorganic metal oxides in 2009.[45] $KCs_2Ga(B_5O_{10})(OH)$ crystallizes in the tetragonal space group $I\bar{4}2d$ (no. 122), and its zeolitic framework $[GaB_5O_{10}]_\infty$ exhibits a totally different topology to that of $Rb_2Ga(B_5O_{10})(H_2O)_4$ (Fig. 1c and f). The asymmetric unit of $KCs_2Ga(B_5O_{10})(OH)$ contains half a Ga atom, half a $[B_5O_{10}]$ cluster, and split alkali metal cations and their disordered coordinated hydroxyl groups. Although the $[GaO_4]$ tetrahedra in $KCs_2Ga(B_5O_{10})(OH)$ are also coordinated with neighbouring four $[B_5O_{10}]$ FBBs, the geometric configuration of the $[GaB_5O_{10}]$ fragment in $KCs_2Ga(B_5O_{10})(OH)$ is different from that in $Rb_2Ga(B_5O_{10})(H_2O)_4$ (Fig. 1a and d). As depicted in Fig. 1e, there are two types of open tunnels (the green and yellow channels) along the [001] direction, while there is another type of open tunnel along the [100] direction (the purple channels). Split alkali metal cations and disordered hydroxyl groups fill these channels. The experimental bandgap of $KCs_2Ga(B_5O_{10})(OH)$ converted from diffuse reflection data using the Kubelka–Munk equation is as large as 6.30 eV, indicating that $KCs_2Ga(B_5O_{10})(OH)$ may have a wide transparency window in the short-wavelength UV spectral region. Powder SHG measurements of $KCs_2Ga(B_5O_{10})(OH)$ demonstrated that it exhibits an enhanced SHG response of about 1.4 times that of KDP.

Barium galloborate $Ba_4Ga[B_{10}O_{18}(OH)_5](H_2O)$ was discovered by Mao *et al.* in 2014.[46] $Ba_4Ga[B_{10}O_{18}(OH)_5](H_2O)$ crystallizes in the polar space group *Cc* (no. 9) and the asymmetric unit of $Ba_4Ga[B_{10}O_{18}(OH)_5](H_2O)$ consists of four Ba cations, one Ga cation, ten boron atoms, twenty-three oxygen atoms, and five hydrogen atoms. Its structure features a three-dimensional $\{Ga[B_{10}O_{18}(OH)_5]\}_\infty$ covalent anionic skeleton composed of $[B_{10}O_{18}(OH)_5]$ FBBs and $[GaO_4]$ tetrahedra joined by Ga–O–B linkages (Fig. 2c). The complex FBB, $[B_{10}O_{18}(OH)_5]$, oligomerized from seven $[BO_4]$ tetrahedra and three $[BO_3]$ triangles, possesses five terminal hydroxyl groups and four exocyclic oxygen atoms for further connections with Ga cations (Fig. 2a). To simplify the structural description, $[B_{10}O_{18}(OH)_5]$ FBB is

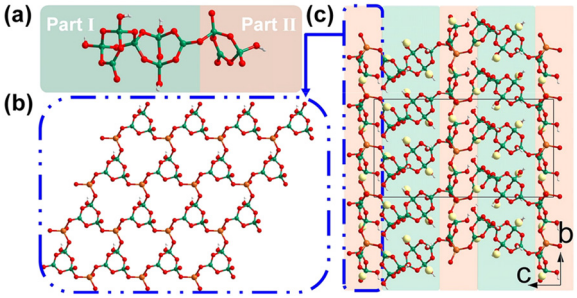

Fig. 2 (a) Complex $[B_{10}O_{18}(OH)_5]$ FBB can be divided into two parts: part 1 $[B_7O_{12}(OH)_4]$ and part 2 $[B_3O_7(OH)]$. (b) Two-dimensional $\{GaO[B_3O_7(OH)]\}_\infty$ layer. (c) Structure of $Ba_4Ga[B_{10}O_{18}(OH)_5](H_2O)$. Ba, Ga, B, O, and H atoms are shown in light yellow, orange, olive, red, and white, respectively.

divided into two parts here (Fig. 2a): part 1 $[B_3O_7(OH)]$ and part 2 $[B_7O_{12}(OH)_4]$. As depicted in Fig. 2b, each $[GaO_4]$ tetrahedron is coordinated with three $[B_3O_7(OH)]$ (part 2) *via* bridging μ_2-O atoms to form a two-dimensional $\{GaO[B_3O_7(OH)]\}_\infty$ layer expanding in the (001) plane. The interlayer $[B_7O_{12}(OH)_4]$ (part 1) linkers connect the adjacent sheets to form the three-dimensional covalent skeleton $\{Ga[B_{10}O_{18}(OH)_5]\}_\infty$ with Ba cations and water molecules filling the vacancies. The diffuse-reflectance absorption spectrum of $Ba_4Ga[B_{10}O_{18}(OH)_5](H_2O)$ indicates that it is transparent in the UV region as its band gap is as large as 4.12 eV. The powder SHG response of $Ba_4Ga[B_{10}O_{18}(OH)_5](H_2O)$ is relatively weak (about 0.2 × KDP@1064 nm), which may be attributed to the low ratio of $[BO_3]$: $\{[BO_4] + [GaO_4]\}$ and the unfavourable arrangement of $[BO_3]$ units.

$Na_4Ga_3B_4O_{12}(OH)$, another alkali metal galloborate incorporating $[BO_3]$ FBBs, was synthesized under surfactant-thermal conditions by Yang *et al.* in 2017.[47] The structure of $Na_4Ga_3B_4O_{12}(OH)$ crystallizes in the noncentrosymmetric cubic space group $F\bar{4}3c$ (no. 219) and its structure features a 3D framework composed of octahedral $[Ga_6(BO_3)_4]$ cages. The octahedral $[Ga_6(BO_3)_4]$ cage is constructed by four $[BO_3]$ triangles and six Ga cations with the $[BO_3]$ triangles capping the four faces and six Ga cations occupying the vertex-sites of octahedron (Fig. 3a). Each $[Ga_6(BO_3)_4]$ cage further connects the neighbouring six cages, thus expanding to an unusual zeolite-topology network $[Ga_3B_4O_{12}(OH)]_\infty$ with disordered Na cations and their coordinated hydroxyl groups filling the cavities (Fig. 3b and c). The experimental band gap (E_g = 4.9 eV) determined from its diffuse-reflectance spectrum indicates that the cut-off edge of $Na_4Ga_3B_4O_{12}(OH)$ is in the short-wavelength UV region. The three principal refractive indices of the crystals belonging to advanced crystal family are equal ($n_1 = n_2 = n_3 = n_0$), even though $Na_4Ga_3B_4O_{12}(OH)$ crystallizes in the noncentrosymmetric space group. This indicates that light waves propagate through crystals in any direction exactly like they would in an isotropic medium, without causing the birefringence phenomenon. This species is not phase-matching and the large dihedral angle between the $[BO_3]$ triangles (70.529°) as

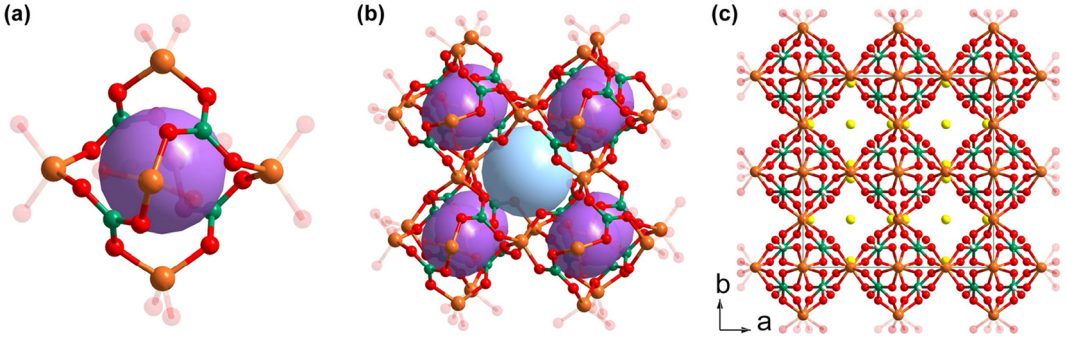

Fig. 3 (a) $[Ga_6(BO_3)_4]$ cage. (b) Cubic cavity (blue ball) constructed from eight $[Ga_6(BO_3)_4]$ cages (purple balls). (c) Structure of $Na_4Ga_3B_4O_{12}(OH)$. Na, Ga, B, O, and H are shown in yellow, orange, olive, and red, respectively.

well as the weak powder SHG response (0.1 × KDP) suggest that $Na_4Ga_3B_4O_{12}(OH)$ may not be a satisfactory NLO crystal.

$LiGa(OH)(BO_3)(H_2O)$ was obtained by Mao *et al.* in 2012, and it is the sole KBBF-like galloborate constructed from two-dimensional layers *via* hydrogen bonding interactions.[43] $LiGa(OH)(BO_3)(H_2O)$ crystallizes in the *P*31*c* (no. 159) space group and there are three kind of basic building units in its structure: triangular $[BO_3]$, tetrahedral hydrated $[LiO_3(H_2O)]$, and $[GaO_3(OH)]$ (Fig. 4a). The assembly of $[BO_3]$, $[LiO_3(H_2O)]$, and $[GaO_3(OH)]$ according to the ratio of 1 : 1 : 1 in the (001) plane give rise to the formation of a two-dimensional $[Li(H_2O)Ga(OH)(BO_3)]_\infty$ layer with coordinated water molecules and hydroxyl groups branched out from the sheet (Fig. 4b). It should be noted that the coordinated water molecules and hydroxyl groups locate in the crystallographic 3-fold axes; therefore, all the hydrogen atoms are disordered, obeying the intrinsic geometric configurations of the hydroxyl group and water molecule, and these terminal units may act as both donors and acceptors of hydrogen bonds. The interlayer O–H···O hydrogen bonds further induce the $[Li(H_2O)Ga(OH)(BO_3)]_\infty$ layers to stack along the [001] directions (Fig. 4c). The

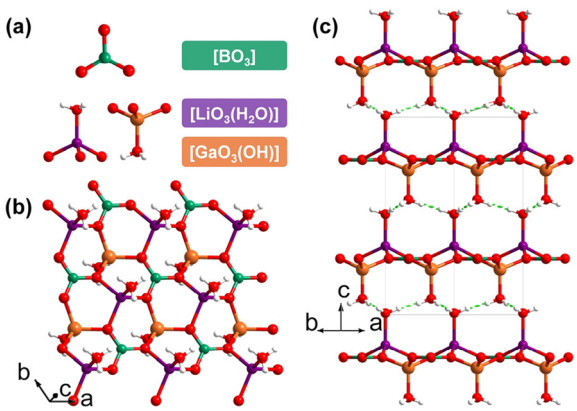

Fig. 4 (a) Three kinds of basic building units ($[BO_3]$, $[LiO_3(H_2O)]$, and $[GaO_3(OH)]$) of $LiGa(OH)(BO_3)(H_2O)$. (b) Two-dimensional $[Li(H_2O)Ga(OH)(BO_3)]_\infty$ layer. (c) Structure of $LiGa(OH)(BO_3)(H_2O)$. Li, Ga, B, O, and H atoms are shown in purple, orange, olive, red, and white, respectively.

functional $[BO_3]$ units are optimally aligned in the lattice and the density of $[BO_3]$ unit (8.22×10^{-3} Å^{-3}) is comparable to that of KBBF (9.42×10^{-3} Å^{-3}), which indicates that an SHG response and a birefringence comparable to that of KBBF could be expected. Unfortunately, further detailed optical properties of this crystal were not reported in the literature due to an unremovable unidentified impurity.

Borates incorporating more than one kind of B–O clusters are rare as they naturally disobey Pauling's 5th rule. The galloborates discussed above contain only one kind of FBB, but there are two cases of hydrated galloborates constructed from two kinds of FBBs.

$Na_5Ga[B_7O_{12}(OH)]_2{\cdot}2B(OH)_3$ was identified as a new NLO crystal by Yang *et al.* in 2022.[41] $Na_5Ga[B_7O_{12}(OH)]_2{\cdot}2B(OH)_3$ crystallizes in the polar *C*2 (no. 5) space group and there are two kinds of FBBs in the lattice: the $[B_7O_{13}(OH)]$ FBB and the isolated $[B(OH)_3]$ cluster (Fig. 5a). The polymerization of $[B_7O_{13}(OH)]$ FBBs along the *b* axis leads to the formation of a one-dimensional $[B_7O_{12}(OH)]_\infty$ chain (Fig. 5b). The $[GaO_4]$ units connect the as-formed chains to form a $\{Ga[B_7O_{12}(OH)]\}_\infty$ layer expanding in the *bc* plane (Fig. 5c). The isolated $[B(OH)_3]$ FBBs are not involved in the $\{Ga[B_7O_{12}(OH)]\}_\infty$ layer, as they as well as the Na cations are located in the voids between adjacent layers and stabilize the whole structure by hydrogen bonds and ionic bonds (Fig. 5d). The experimental data of $Na_5Ga[B_7O_{12}(OH)]_2{\cdot}2B(OH)_3$ showed a relatively small band gap as large as 3.90 eV but a remarkable powder SHG intensity. The extremely large powder SHG response of $Na_5Ga[B_7O_{12}(OH)]_2{\cdot}2B(OH)_3$ (as large as 4.6 times that of KDP) is a record in galloborate systems. $Na_5Ga[B_7O_{12}(OH)]_2{\cdot}2B(OH)_3$ is phase-matching according to the Kurtz–Perry rules.

$Ba_3Ga_2[B_3O_6(OH)]_2[B_4O_7(OH)_2]$ is another NLO-active galloborate constructed by two kinds of FBBs (Fig. 6a).[48] This species was found and identified by Yang *et al.* in 2013 for the first time. $Ba_3Ga_2[B_3O_6(OH)]_2[B_4O_7(OH)_2]$ crystallizes in the polar space group *Fdd*2 (no. 43), and it features a sandwich $\{Ga_2[B_3O_6(OH)]_2[B_4O_7(OH)_2]\}_\infty$ layer. Each sandwich $\{Ga_2[B_3O_6(OH)]_2[B_4O_7(OH)_2]\}_\infty$ layer can be divided into two $[GaOB_3O_6(OH)]_\infty$ single layer and $[B_4O_7(OH)_2]$ linkages

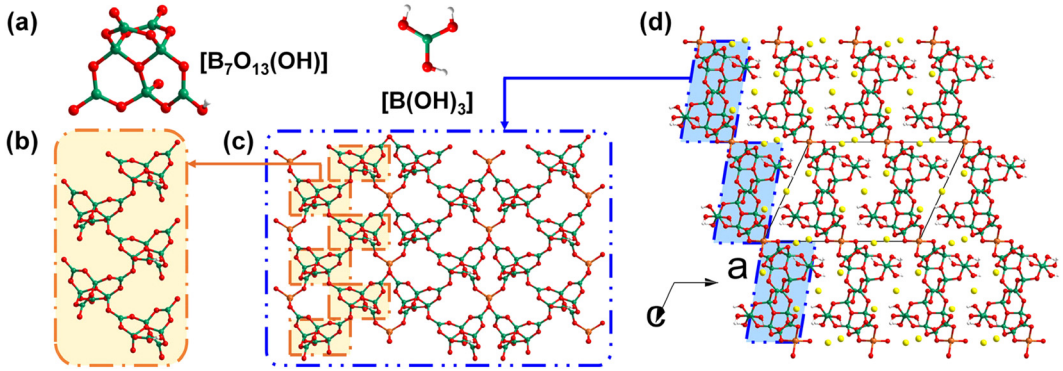

Fig. 5 (a) $[B_7O_{13}(OH)]$ FBB and $[B(OH)_3]$ FBB. (b) One-dimensional $[B_7O_{12}(OH)]_\infty$ chain. (c) Two-dimensional $\{Ga[B_7O_{12}(OH)]\}_\infty$ layer. (d) Structure of $Na_5Ga[B_7O_{12}(OH)]_2{\cdot}2B(OH)_3$. Na, Ga, B, O, and H atoms are shown in yellow, orange, olive, red, and white, respectively.

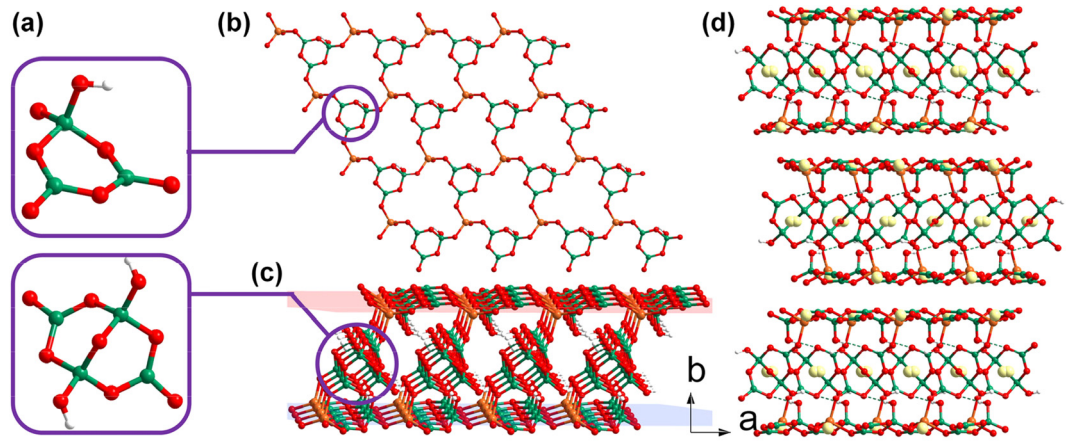

Fig. 6 (a) $[B_3O_6(OH)]$ FBB and $[B_4O_7(OH)_2]$ FBB. (b) Two-dimensional $[GaOB_3O_6(OH)]_\infty$ single layer. (c) Complex $\{Ga_2[B_3O_6(OH)]_2[B_4O_7(OH)_2]\}_\infty$ layer. (d) Structure of $Ba_3Ga_2[B_3O_6(OH)]_2[B_4O_7(OH)_2]$. Ba, Ga, B, O, and H atoms are shown in yellow, orange, olive, red, and white, respectively.

(Fig. 6c). As shown in Fig. 6b, only $[B_3O_6(OH)]$ FBBs as well as the $[GaO_4]$ tetrahedra are involved in constructing the $[GaOB_3O_6(OH)]_\infty$ single layer with embedded eighteen-membered rings (18-MRs). A pair of $[GaOB_3O_6(OH)]_\infty$ single layers are assembled into one sandwich layer through the bridging $[B_4O_7(OH)_2]$ FBBs. Apart from the Ga–O ionic bonding interaction, the hydrogen bonds between two kinds of FBBs also help to stabilize the whole sandwich layer. As shown in Fig. 6d, Ba cations are located within and between the sandwiched layers to balance the charge and expand the two-dimensional layer to a three-dimensional framework. Interestingly, $Ba_3Ga_2[B_3O_6(OH)]_2[B_4O_7(OH)_2]$ is isostructural with its Al counterpart. The Ba cations in the structure of $Ba_3Ga_2[B_3O_6(OH)]_2[B_4O_7(OH)_2]$ are disordered (Fig. 6d) while the Ba cations in the structure of $Ba_3Al_2[B_3O_6(OH)]_2[B_4O_7(OH)_2]$ are ordered. The large SHG response (3.0 × KDP@1064 nm) and the band gap (E_g = 5.0 eV) are comparable to $Ba_3Al_2[B_3O_6(OH)]_2[B_4O_7(OH)_2]$ (3.0 × KDP@1064 nm, E_g = 5.4 eV), as can be inferred from their highly similar structures. The excellent optical properties indicate that $Ba_3Ga_2[B_3O_6(OH)]_2[B_4O_7(OH)_2]$ may be a potential NLO crystal in the UV region.

3. Alkali/alkaline earth metal galloborate halides

The first galloborate halide $NaBa_4(GaB_4O_9)_2Cl_3$ was synthesized by Li *et al.* in 2006, and its structure was determined by powder X-ray diffraction data.[49] $NaBa_4(GaB_4O_9)_2Cl_3$ is a salt-inclusion galloborate, which shows a $[GaB_4O_9]$ network featuring the *dia* topology. It is formed by the interconnection of $[B_4O_9]$ FBBs and $[GaO_4]$ tetrahedra with Ba cations, Cl ions, and NaCl salt filling the tunnels. Soon after the discovery of $NaBa_4(GaB_4O_9)_2Cl_3$, Barbier reported three isostructural borate halides, namely $Ba_2TB_4O_9Cl$ (T = Al and Ga) and $Ba_2GaB_4O_9Br$, whose structures are similar with $NaBa_4(GaB_4O_9)_2Cl_3$.[50] Noncentrosymmetric $NaBa_4(AlB_4O_9)_2X_3$ (X = Cl and Br) was synthesized by Wang *et al.* and Pan *et al.* in 2012 to 2013.[51,52] In 2016, the single crystals of $NaBa_4(GaB_4O_9)_2X_3$ (X = Cl and

Br) were successfully obtained by Pan *et al.*[53] Moreover, Pan *et al.* also identified [GaO_4] as an NLO-active unit for the first time. The mentioned tetraborates show the same [GaB_4O_9] anionic skeleton featuring the *dia* topology with salt components incorporated.

Since $Ba_2GaB_4O_9Cl$ and $Ba_2GaB_4O_9Br$ are isostructural, only the structure of $Ba_2GaB_4O_9Cl$ is discussed here. $Ba_2GaB_4O_9Cl$ crystallizes in the $P4_2nm$ space group (no. 102). All the [GaO_4] tetrahedra in the structure are four-coordinated (Fig. 7a), and the alternative arrangement of Ga cations and B–O clusters gives rise to a zeolite-like anionic framework with the *dia* topology (Fig. 7c and d). There are two kinds of channels incorporated in the $[GaB_4O_9]_\infty$ anionic skeleton for encapsulation of the salt components (see the blue and purple pipes in Fig. 7b, c and e). $Ba_2GaB_4O_9Cl$ has a moderate SHG effect (about 1.0 × KDP@1064 nm), while the powder SHG response of $Ba_2GaB_4O_9Br$ has not yet been reported.

Both $NaBa_4(GaB_4O_9)_2Cl_3$ and $NaBa_4(GaB_4O_9)_2Br_3$ crystallize in the $P42nm$ space group (no. 102), and their structures are similar to that of $Ba_2GaB_4O_9Cl$ with different included salts. The Ba cations, Cl ions, and NaCl salt make up a ionic bonding network filling the tunnels in the $[GaB_4O_9]_\infty$ anionic skeleton (Fig. 7c and f). Although Ga^{3+} and Al^{3+} cations have similar outer electronic configurations, the 3d electrons of Ga^{3+} cations as well as the reduced ability of dangling bond elimination narrows the band gaps of galloborates compared with isostructural aluminoborates. $NaBa_4(GaB_4O_9)_2Cl_3$ and $NaBa_4(GaB_4O_9)_2Br_3$ show narrowed band gaps (3.76 and 3.71 eV) compared with the band gaps of their aluminium counterparts (3.93 and 3.95 eV). Whereas $NaBa_4(GaB_4O_9)_2Cl_3$ and $NaBa_4(GaB_4O_9)_2Br_3$ show enhanced powder SHG responses as large as 1.5 times and 1.1 times that of KDP under 1064 nm fundamental laser radiation, the SHG responses of $NaBa_4(AlB_4O_9)_2X_3$ (X = Cl and Br) are 0.9 times and 0.8 times that of KDP, respectively. Theoretical calculations illustrated that the Ga–O hybrid orbitals also contribute to the optical properties and thus verify that the [GaO_4] non-π conjugated is also an NLO-active chromophore.

In 2013, Li *et al.* synthesized a mixed metal galloborate $K_2Ba_4Ga_4Li_2B_6O_{21}$ by spontaneous crystallization with K_2O–B_2O_3–LiF flux.[54] $K_2Ba_4Ga_4Li_2B_6O_{21}$ can be regarded as the result of chemical co-substitution from the parental $K_2Al_2B_2O_7$ and its formula is consistent with the triple $K_2Al_2B_2O_7$ ($K_6Al_6B_6O_{21}$). Covalent [LiO_4] and [GaO_4] tetrahedra act as 4-connected linkages, like [AlO_4] in $K_2Al_2B_2O_7$. The polymerization of [LiO_4], [GaO_4], and [BO_3] in the (001) plane leads to the formation of the three-dimensional $[Ga_4Li_2B_6O_{21}]_\infty$ framework. The UV–Vis diffuse-reflectance spectrum shows that the cut-off edge of $K_2Ba_4Ga_4Li_2B_6O_{21}$ is about 226 nm. The structure of $K_2Ba_4Ga_4Li_2B_6O_{21}$ is seriously disordered (Fig. 8), and the powder SHG response of $K_2Ba_4Ga_4Li_2B_6O_{21}$ is as large as only half that of KDP.

Inspired by the discovery of $K_2Ba_4Ga_4Li_2B_6O_{21}$, a series of aluminoborate fluorides and galloborate fluorides ($A_3Ba_3Li_2T_4B_6O_{20}F$, A = K or Rb, T = Al or Ga) with similar formulas were synthesized and identified as NLO crystals.[55–57] $K_3Ba_3Li_2Ga_4B_6O_{20}F$ and $Rb_3Ba_3Li_2Ga_4B_6O_{20}F$ were synthesized by Xia *et al.* in 2018, after the discovery of $K_3Ba_3Li_2Al_4B_6O_{20}F$ and $Rb_3Ba_3Li_2Al_4B_6O_{20}F$. Although galloborate fluorides $A_3Ba_3Li_2Ga_4B_6O_{20}F$ (A = K and Rb) possess a similar formula to the aluminoborate fluorides $A_3Ba_3Li_2Ga_4B_6O_{20}F$ (A = K and Rb), they cannot be regarded as the results of a simple chemi-

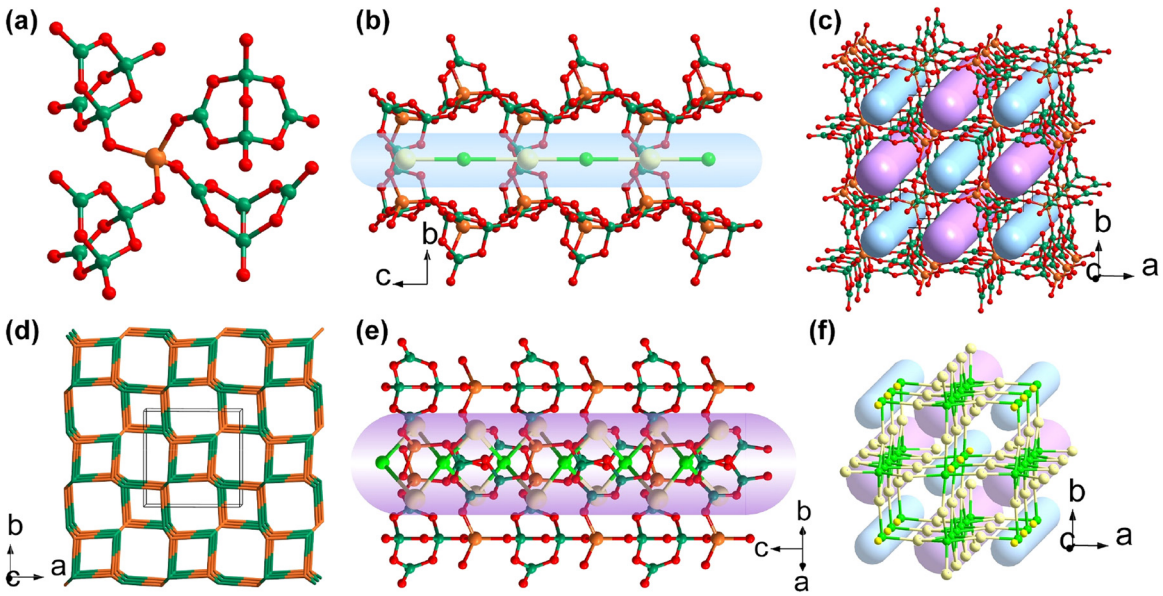

Fig. 7 (a) Coordination environment of Ga cations. (b) One-dimensional channel containing $[BaCl]_\infty$ chains. (c) Three-dimensional $[GaB_4O_9]_\infty$ anionic skeleton. (d) The *dia* topology of $Ba_2GaB_4O_9Cl$ and $NaBa_4(GaB_4O_9)_2X_3$ (X = Cl, Br). (e) One-dimensional channels containing $[Ba_2Cl]_\infty$ chains. (f) $[NaCl]_\infty$ and $[Ba_2Cl]_\infty$ chains filling the two kinds of channels of the $[GaB_4O_9]_\infty$ anionic skeleton. Na, Ba, Ga, B, O, and H atoms are shown in yellow, light yellow, orange, olive, red, white, and green, respectively.

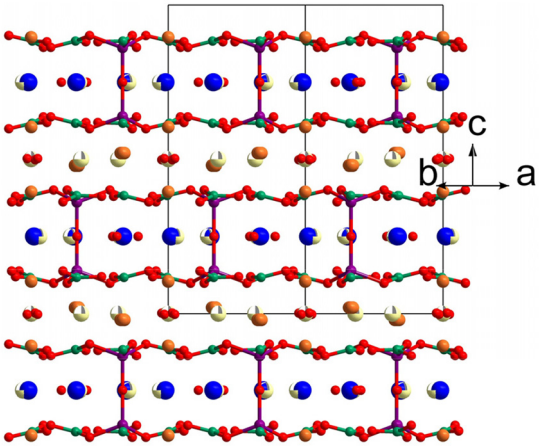

Fig. 8 Structure of $K_2Ba_4Li_2Ga_4B_6O_{21}$. K, Ba, Li, Ga, B, and O atoms are shown in blue, light yellow, purple, orange, olive, and red, respectively.

cal substitution of $[AlO_4]$ by $[GaO_4]$ tetrahedra. $A_3Ba_3Li_2Al_4B_6O_{20}F$ (A = K and Rb) features a double-layered $[Li_2Al_4B_6O_{20}F]_\infty$ sheet (Fig. 9a) while the anionic skeleton of $A_3Ba_3Li_2Ga_4B_6O_{20}F$ (A = K and Rb) is the three-dimensional $[Ga_4Li_2B_6O_{20}F]_\infty$ framework (Fig. 9b). The different orientations of covalent $[LiO_4]$ and $[AlO_4]/[GaO_4]$ are responsible for the different dimensionalities of $[Li_2Al_4B_6O_{20}F]_\infty$ and $[Ga_4Li_2B_6O_{20}F]_\infty$. The $[LiO_4]$ and $[AlO_4]$ tetrahedra marked with yellow arrows face the same positions and are coordinated with $[BO_3]$ triangles to form the $[Li_2Al_4B_6O_{20}F]_\infty$ double layer, whereas the $[LiO_4]$ and $[AlO_4]$ tetrahedra marked with yellow and blue arrows face opposite positions to expand the layered structure to a three-dimensional framework, as depicted in Fig. 9c and d. The weakened powder SHG responses of $A_3Ba_3Li_2Ga_4B_6O_{20}F$ (A = K and Rb) were 0.7 and 0.5 times that of KDP, which are smaller than that of $A_3Ba_3Li_2Al_4B_6O_{20}F$ (A = K and Rb) (1.5 × KDP@1064 nm). The calculated birefringence values were 0.0416 and 0.0434@800 nm, respectively.

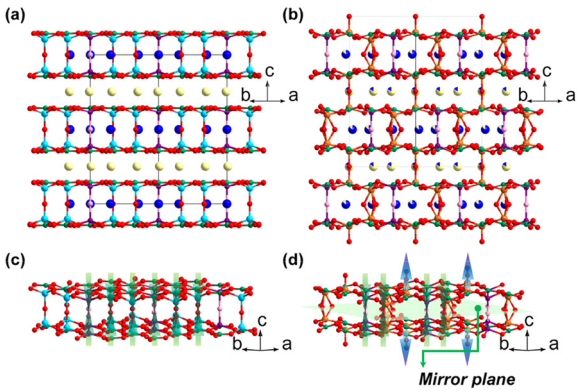

Fig. 9 (a) Structure of $KBa_3Li_2Al_4B_6O_{20}F$. (b) Structure of $KBa_3Li_2Ga_4B_6O_{20}F$. (c) Double-layered $[Li_2Al_4B_6O_{20}F]_\infty$ sheet. (d) Double-layered $[Li_2Ga_4B_6O_{20}F]_\infty$ sheet. K, Ba, Li, Al, Ga, B, O, and F atoms are shown in blue, light yellow, purple, light blue, orange, olive, red, and pink, respectively.

4. Summary and perspectives

This frontier article focused on the recent progress of NLO inorganic galloborates. These galloborates are divided into two types, namely alkali/alkaline earth metal galloborates and alkali/alkaline earth metal galloborate halides, in terms of their compositions. Their chemical formulas, space groups, anionic structural features, SHG intensities, and band gaps are summarized. New raw materials and synthetic methods are used to obtain new galloborates. For example, gallium isopropoxide and the surfactant–thermal method are used in the synthetic process. In these galloborates, $KCs_2Ga(B_5O_{10})(OH)$ shows the shortest cut-off edge of 190 nm, while $Na_5Ga[B_7O_{12}(OH)]_2{\cdot}2B(OH)_3$ shows the largest SHG effect of 4.6 × KDP. Although some progress has been achieved, the development of NLO galloborates is still in the primary stage, and some aspects need further study.

It is noteworthy that only the $[GaO_4]$ configuration has been observed in these NLO galloborates. Ga cations have several other coordination geometries, such as square pyramid, trigonal bipyramidal, and octahedron. It is expected that noncentrosymmetric galloborates could be obtained by the combination of $[GaO_5]/[GaO_6]$ with borate anionic units. The fluorination strategy has been widely used to obtain new NLO crystals. Two NLO alkali/alkaline earth metal galloborate fluorides with enlarged band gaps have been reported, where the introduction of fluoride ions greatly widens the transparency windows in the short-wavelength spectral region. In these two compounds, fluorine ions are only coordinated with alkali/alkaline earth metal cations. Neither $[GaO_mF_n]$ ($m + n$ = 4, 5, 6) nor $[BO_xF_{4-x}]$ (x = 1, 2, 3) units are observed in these NLO galloborates. Galloborates with larger SHG effects, and shorter cut-off edges are expected if these NLO-active units can be realized in the future. It should be noted that emergent boron-based compounds with other anionic units, like $[NO_3]$, $[CO_3]$, $[SO_4]$, $[PO_4]$, $[GeO_4]$, and $[SiO_4]$, will accelerate the exploration of new NLO crystals.[58–63] Finally, it is important to grow large single crystals for practical applications. Compared with aluminoborates, the general raw material of Ga_2O_3 possesses a lower melting point, and the viscosity of the corresponding melts are also reduced, which are favourable to crystal growth. We believe the structural diversity of galloborates will inspire the design of more functional NLO crystals in future work.

Data availability

No primary research results, software or code have been included and no new data were generated or analysed as part of this review.

Conflicts of interest

There are no conflicts to declare.

Acknowledgements

This work was supported by the National Natural Science Foundation of China (Grant 21975224).

References

1 M. Mutailipu, K. R. Poeppelmeier and S. L. Pan, *Chem. Rev.*, 2021, **121**, 1130–1202.
2 P. S. Halasyamani and W. G. Zhang, *Inorg. Chem.*, 2017, **56**, 12077–12085.
3 J. Chen, C. L. Hu, F. Kong and J. G. Mao, *Acc. Chem. Res.*, 2021, **54**, 2775–2783.
4 Y. Q. Li, J. H. Luo and S. G. Zhao, *Acc. Chem. Res.*, 2022, **55**, 3460–3469.
5 L. Kang and Z. S. Lin, *Light: Sci. Appl.*, 2022, **11**, 201.
6 M. Mutailipu, Z. H. Yang and S. L. Pan, *Acc. Mater. Res.*, 2021, **2**, 282–291.
7 Q. X. Liu, Q. Wu, T. Y. Wang, L. Kang, Z. S. Lin, Y. G. Wang and M. J. Xia, *Chin. J. Struct. Chem.*, 2023, **42**, 100026.
8 H. A. Liu, H. P. Wu, Z. G. Hu, J. Y. Wang, Y. C. Wu and H. W. Yu, *J. Am. Chem. Soc.*, 2023, **145**, 12691–12700.
9 C. C. Jin, H. Zeng, F. Zhang, H. T. Qiu, Z. H. Yang, M. Mutailipu and S. L. Pan, *Chem. Mater.*, 2022, **34**, 440–450.
10 J. H. Liu, M. H. Lee, C. X. Li, X. H. Meng and J. Y. Yao, *Inorg. Chem.*, 2022, **61**, 19302–19308.
11 X. Y. Li, J. H. Li, J. W. Cheng and G. Y. Yang, *Inorg. Chem.*, 2023, **62**, 1264–1271.
12 Y. N. Zhang, Q. F. Li, B. B. Chen, Y. Z. Lan, J. W. Cheng and G. Y. Yang, *Inorg. Chem. Front.*, 2022, **9**, 5032–5038.
13 H. T. Qiu, F. M. Li, C. C. Jin, Z. H. Yang, J. J. Li, S. L. Pan and M. Mutailipu, *Angew. Chem., Int. Ed.*, 2024, **63**, e202316194.
14 X. Liu, Y. C. Yang, M. Y. Li, L. Chen and L. M. Wu, *Chem. Soc. Rev.*, 2023, **52**, 8699–8720.
15 J. J. Li, W. F. Chen, Y. Z. Lan and J. W. Cheng, *Molecules*, 2023, **28**, 5068.
16 W. F. Zhou and S. P. Guo, *Acc. Chem. Res.*, 2024, **57**, 648–660.
17 H. X. Fan, N. Ye and M. Luo, *Acc. Chem. Res.*, 2023, **56**, 3099–3109.
18 C. T. Chen, Y. C. Wu, A. D. Jiang, B. C. Wu, G. M. You, R. K. Li and S. J. Lin, *J. Opt. Soc. Am. B*, 1989, **6**, 616–621.
19 C. T. Chen, B. C. Wu, A. D. Jiang and G. M. You, *Sci. Sin., Ser. B*, 1985, **28**, 235–243.
20 B. C. Wu, D. Y. Tang, N. Ye and C. T. Chen, *Opt. Mater.*, 1996, **5**, 105–109.
21 Q. Wei, J. W. Cheng, C. He and G. Y. Yang, *Inorg. Chem.*, 2014, **53**, 11757–11763.
22 W. F. Chen, J. Y. Lu, J. J. Li, Y. Z. Lan, J. W. Cheng and G. Y. Yang, *Chem. – Eur. J.*, 2024, **30**, e202400739.
23 J. H. Huang, C. C. Jin, P. L. Xu, P. F. Gong, Z. S. Lin, J. W. Cheng and G. Y. Yang, *Inorg. Chem.*, 2019, **58**, 1755–1758.
24 W. Z. Zhao, Y. N. Zhang, Y. Z. Lan, J. W. Cheng and G. Y. Yang, *Inorg. Chem.*, 2022, **61**, 4246–4250.
25 Q. Wei, J. J. Wang, C. He, J. W. Cheng and G. Y. Yang, *Chem. – Eur. J.*, 2016, **22**, 10759–10762.
26 F. H. Ding, K. J. Griffith, W. G. Zhang, S. X. Cui, C. Zhang, Y. R. Wang, K. Kamp, H. W. Yu, P. S. Halasyamani, Z. H. Yang, S. L. Pan and K. R. Poeppelmeier, *J. Am. Chem. Soc.*, 2023, **145**, 4928–4933.
27 T. Ouyang, Y. G. Shen and S. G. Zhao, *Chin. J. Struct. Chem.*, 2023, **42**, 100024.
28 W. J. Xie, R. L. Tang, S. N. Yan, N. Ma, C. L. Hu and J. G. Mao, *Small*, 2023, 2307072.
29 M. Cheng, X. L. Hou, Z. H. Yang and S. L. Pan, *Mater. Chem. Front.*, 2023, **7**, 4683–4692.
30 M. Mutailipu and S. L. Pan, *Angew. Chem., Int. Ed.*, 2020, **59**, 20302–20317.
31 H. K. Su, Z. T. Yan, X. L. Hou and M. Zhang, *Chin. J. Struct. Chem.*, 2023, **42**, 100027.
32 G. Q. Shi, Y. Wang, F. F. Zhang, B. B. Zhang, Z. H. Yang, X. L. Hou, S. L. Pan and K. R. Poeppelmeier, *J. Am. Chem. Soc.*, 2017, **139**, 10645–10648.
33 C. M. Huang, M. Mutailipu, F. F. Zhang, K. J. Griffith, C. Hu, Z. H. Yang, J. M. Griffin, K. R. Poeppelmeier and S. L. Pan, *Nat. Commun.*, 2021, **12**, 2597.
34 J. H. Jiao, M. Zhang and S. L. Pan, *Angew. Chem., Int. Ed.*, 2023, **62**, e2022170.
35 Q. F. Li, W. F. Chen, Y. Z. Lan and J. W. Cheng, *Chin. J. Struct. Chem.*, 2023, **42**, 100036.
36 X. F. Wang, F. F. Zhang, L. Gao, Z. H. Yang and S. L. Pan, *Adv. Sci.*, 2019, **6**, 1901679.
37 H. W. Yu, H. P. Wu, S. L. Pan, Z. H. Yang, X. L. Hou, X. Su, Q. Jing, K. R. Poeppelmeier and J. M. Rondinelli, *J. Am. Chem. Soc.*, 2014, **136**, 1264–1267.
38 T. T. Tran, N. Z. Koocher, J. M. Rondinelli and P. S. Halasyamani, *Angew. Chem., Int. Ed.*, 2017, **56**, 2969–2973.
39 H. K. Liu, Y. Wang, B. B. Zhang, Z. H. Yang and S. L. Pan, *Chem. Sci.*, 2020, **11**, 694–698.
40 W. F. Liu, C. A. Chen, X. Y. Li and G. Y. Yang, *Cryst. Growth Des.*, 2023, **23**, 3556–3561.
41 C. A. Chen, W. F. Liu and G. Y. Yang, *Chem. Commun.*, 2022, **58**, 8718–8721.
42 Z. H. Liu, P. Yang and P. Li, *Inorg. Chem.*, 2007, **46**, 2965–2967.
43 T. Hu, C. L. Hu, F. Kong, J. G. Mao and T. C. W. Mak, *Inorg. Chem.*, 2012, **51**, 8810–8817.
44 L. Cheng and G. Y. Yang, *Inorg. Chem.*, 2018, **57**, 13505–13512.
45 C. Rong, Z. W. Yu, Q. Wang, S. T. Zheng, C. Y. Pan, F. Deng and G. Y. Yang, *Inorg. Chem.*, 2009, **48**, 3650–3659.
46 H. Yang, C. L. Hu, J. L. Song and J. G. Mao, *RSC Adv.*, 2014, **4**, 45258–45265.
47 S. J. Yu, X. Y. Gu, T. T. Deng, J. H. Huang, J. W. Cheng and G. Y. Yang, *Inorg. Chem.*, 2017, **56**, 12695–12698.
48 L. Cheng, Q. Wei, H. Q. Wu, L. J. Zhou and G. Y. Yang, *Chem. – Eur. J.*, 2013, **19**, 17662–17667.

49 R. K. Li and Y. Yu, *Inorg. Chem.*, 2006, **45**, 6840–6843.
50 J. Barbier, *Solid State Sci.*, 2007, **9**, 344–350.
51 J. X. Zhang, S. F. Zhang, Y. C. Wu and J. Y. Wang, *Inorg. Chem.*, 2012, **51**, 6682–6686.
52 H. W. Yu, S. L. Pan, H. P. Wu, Z. H. Yang, L. Y. Dong, X. Su, B. B. Zhang and H. Y. Li, *Cryst. Growth Des.*, 2013, **13**, 3514–3521.
53 M. Wen, X. Su, H. P. Wu, J. J. Lu, Z. H. Yang and S. L. Pan, *J. Phys. Chem. C*, 2016, **120**, 6190–6197.
54 X. Gao and R. K. Li, *Opt. Mater.*, 2014, **36**, 2026–2029.
55 X. H. Meng, F. Liang, M. J. Xia and Z. S. Lin, *Inorg. Chem.*, 2018, **57**, 5669–5676.
56 S. G. Zhao, L. Kang, Y. G. Shen, X. D. Wang, M. A. Asghar, Z. S. Lin, Y. Y. Xu, S. Y. Zeng, M. C. Hong and J. H. Luo, *J. Am. Chem. Soc.*, 2016, **138**, 2961–2964.
57 H. P. Wu, H. W. Yu, S. L. Pan and P. S. Halasyamani, *Inorg. Chem.*, 2017, **56**, 8755–8758.
58 L. Y. Zhang, S. B. Wang, F. F. Zhang, Z. H. Yang and X. L. Hou, *Dalton Trans.*, 2023, **52**, 13492–13496.
59 S. Bai, D. Q. Yang, B. B. Zhang, L. Li and Y. Wang, *Dalton Trans.*, 2022, **51**, 3421–3425.
60 W. F. Chen, M. J. Zou, J. J. Li, Y. N. Zhang, Y. Z. Lan, J. W. Cheng and G. Y. Yang, *Inorg. Chem.*, 2024, **63**, 9026–9030.
61 J. Bruns, H. A. Höppe, M. Daub, H. Hillebrecht and H. Huppertz, *Chem. – Eur. J.*, 2020, **26**, 7966–7980.
62 R. Pan, J. W. Cheng, B. F. Yang and G. Y. Yang, *Inorg. Chem.*, 2017, **56**, 2371–2374.
63 W. J. Xie, C. L. Hu, Z. Fang, M. Y. Cao, Y. Lin and J. G. Mao, *Inorg. Chem.*, 2022, **61**, 10629–10633.